ELSEVIER

Journal of Nuclear Materials 317 (2003) 13–31

journal of nuclear materials

www.elsevier.com/locate/jnucmat

Evolution of fine-scale defects in stainless steels neutron-irradiated at 275 °C

D.J. Edwards *, E.P. Simonen, S.M. Bruemmer

Pacific Northwest National Laboratory, Materials Interfaces and Characterization Group, Structural Materials Development, MSIN P8-15 Richland, WA 99352, USA

Received 15 January 2002; accepted 26 November 2002

Abstract

Six austenitic stainless steel heats (three heats each of 304SS and 316SS) neutron-irradiated at 275 °C from 0.6 to 13.3 dpa have been carefully characterized by TEM and their hardness measured as a function of dose. The characterization revealed that the microstructure is dominated by a very high density of small Frank loops present in sizes as small as 1 nm and perhaps lower, which could be of both vacancy and interstitial-type. Frank loop density saturated at the lowest doses characterized, whereas the Frank loop size distributions changed with increasing dose from an initially narrow, symmetric shape to a broader, asymmetric shape. Although substantial hardening is caused by the small defects, a simple correlation between hardness changes and density and size of defects does not exist. These results indicate that radiation-induced segregation to the Frank loops could play a role in both defect evolution and hardening response.

1. Introduction

Austenitic stainless steels are a common structural material used in current generation light water reactor (LWR) components as well as future reactor concepts. The radiation environment in these reactors causes substantial degradation in the properties of the stainless steel that can lead to premature failure. The changes in properties derive from the cascade damage produced by the high-energy neutrons that introduce both interstitial and vacancy-type point defects and clusters into the metal lattice. The migration and interaction of these defects and their clusters induce changes in the mechanical and physical properties of the material as well as the matrix microstructure and the grain boundary microchemistry. Radiation hardening and a concomitant ductility loss, irradiation-assisted stress corrosion cracking (IASCC), void swelling and precipitation represent the severe consequences of neutron irradiation.

While extensive studies have been conducted on austenitic stainless steels over the past few decades, much of this work was done under the auspices of the breeder reactor programs in the 1970s and 1980s and more recently in the fusion reactor materials research programs. Many of the experiments focused on irradiation temperatures and doses that were different than those of interest to the LWR community. Reviews by Maziasz [1], Zinkle et al. [2] and more recently by Bruemmer et al. [3] and Rowcliffe et al. [4] summarize much of our understanding on the microstructural evolution gained from those early experiments, which spanned the temperature range from 50 to 700 °C. The review by Bruemmer et al. [3] focused on addressing the current understanding of radiation effects in stainless steels as it pertained to IASCC in LWRs, a phenomenon involving components irradiated at temperatures near 290 °C. This range of irradiation temperatures (50–700 °C) spans a critical temperature regime for irradiated stainless steels in that at ~300 °C, the stability of

* Corresponding author. Tel.: +1-509 376 4867; fax: +1-509 376 0418.

E-mail address: dan.edwards@pnl.gov (D.J. Edwards).

0022-3115/03/$ - see front matter © 2003 Elsevier Science B.V. All rights reserved.
doi:10.1016/S0022-3115(03)00002-3

vacancy-type defects changes in such a manner that the onset of void swelling and significant radiation-induced precipitation occurs. This temperature represents the annealing stage V, above which vacancy clusters become thermally unstable and begin to emit vacancies into the lattice [2,4]. The microstructure of stainless steels irradiated below ~300 °C evolves differently than that of stainless steels irradiated above this transition temperature, most notably in that no voids have been found below this temperature, only small defect clusters, dislocation loops and some fine-scale precipitation. According to Maziasz, there is limited evidence to suggest that a high density of ultra-fine He bubbles can form in a high density below irradiation temperatures of ~300 °C, but this may require doses of several displacements per atom (dpa) to occur.

All of these reviews conclude that the radiation-induced microstructure in stainless steels irradiated below Stage V is best described as a mixture of 'black spot' damage and Frank loops (faulted loops with $\mathbf{b} = a_o/3\langle 111\rangle$). In his review Maziasz indicates that the Frank loops can appear as 'black spots' when they are very small (2–3) nm, but in later reviews this distinction has seemingly been lost and the character of the black spots is often considered as distinct from the larger Frank loops. Though the data appears to be limited in detail for $T_{irr} < 300$ °C, the density of the black spots saturates around $2\text{–}4 \times 10^{23}$ m^{-3} and the Frank loops somewhat lower. The black spots are usually less than a 5 nm in diameter, whereas the Frank loops approach sizes up to 40 nm. As the irradiation temperature increases above 300 °C, the black spots decrease in density whereas the Frank loops and line dislocations become the dominant dislocation-type defect. The Frank loops under these conditions are much larger, growing to diameters of 200 nm or larger at irradiation temperatures of 360 °C or higher with a density that decreases rapidly above 400 °C. The microstructure at these temperatures is further complicated by the presence of He bubbles, voids and radiation-induced precipitation. Though the review by Zinkle et al. [2] indicated that below Stage V radiation-induced segregation (RIS) is minimal, considerable research has demonstrated that RIS exists at an appreciable level near 290 °C and likely exists at even lower irradiation temperatures. Bruemmer et al. [3] discussed this topic in their review of IASCC in irradiated stainless steels.

The nature of the black spots is one issue that remains unclear and has important implications regarding the interpretation of the microstructural evolution in austenitic stainless steels. While Frank loops larger than 10 nm have been shown to be interstitial loops at irradiation temperatures above 360 °C [5–8], this apparently has never been demonstrated for the much smaller Frank loops that exist at lower irradiation temperatures, particularly below ~300 °C. This is not an easy task, primarily because of the small size of the loops that are typically less than 10 nm in average size. Loops in this size range require a very careful and laborious analysis of the strain field contrast to determine their true character. A further complication is that many of the studies involve a range of irradiation conditions (proton, electron or neutron irradiation), thin foil versus bulk irradiation experiments, and different alloys and impurity contents. For the purposes of this paper, the brief review given below will concentrate only upon stainless steels irradiated under cascade damage conditions, that is, the results of 1 MeV electron irradiation experiments will not be included.

For irradiation temperatures less than ~300 °C, the general tendency is to accept that that the visible Frank loops represent the interstitial component of the microstructure, whereas the unidentified black spot damage is thought to be predominantly vacancy in nature, perhaps stacking fault tetrahedra (SFT) as observed by Horiki and Kiritani [9] in a ternary FeCrNi alloy. Horiki and Kiritani suggested that the small SFTs they observed were formed directly from the cascade collapse. An important point to recognize is that the SFTs observed by Horiki and Kiritani were found in a Fe–16wt%Ni–15wt%Cr ternary alloy with low levels of impurities, quite different from the commercial stainless steels often studied in other work. Maziasz [1] and Zinkle et al. [2] both concluded separately in their reviews that SFT are present in very low densities, comprising less than 1% of the visible defect population. Their reviews, however, are of experimental studies on alloys closer to a commercial nature, not pure ternary FeCrNi alloys.

Other more recent studies also make the point that the microstructure is comprised of both black spots and interstitial Frank loops [10–21], but the black spots are not identified as to their nature and the Frank loops are often assumed to be interstitial-type loops. Dai et al. [15] reported that 304L irradiated with 800 MeV protons contained both SFT and Frank loops, but the SFT (of mean size 1.5 nm) comprised only 20–25% of the visible defects and their density and mean size did not change with increasing dose. In a separate irradiation experiment on four of the heats irradiated in this study, Bailat et al. [16,17] reported loop densities on the order of $\sim 1.7\text{–}3 \times 10^{23}$ m^{-3}, but did not describe in detail the nature of the loops. Most recently, Edwards et al. [20,21] presented limited evidence in LWR-irradiated stainless steels that black spots are in fact small Frank loops indistinguishable from the larger Frank loops when using a technique that images the stacking fault of the loops. This issue needs to be further explored in order to reconcile the differences among various experiments and more accurately relate the changes in microstructure to the observed changes in properties of the irradiated stainless steels.

In the following sections, the results of a systematic characterization of LWR-irradiated 316SS and 304SS heats are presented. Details of the evolution of defects that occur at doses from ~1 to 13 dpa during irradiation at 275 °C will be presented, as well as the accompanying change in hardness at room temperature and 275 °C. The importance of the microstructural features are discussed relative to our understanding of radiation damage, radiation hardening and possible impurity effects.

2. Experimental

Six austenitic stainless steel heats were irradiated at an in-core position at 275 °C (in the contact with coolant water) in the Barsebäck reactor. The samples were in the form of constant extension rate tensile (CERT) specimens used for post-irradiation stress corrosion cracking testing at 275 °C, the details of which have been reported by Jenssen et al. [22,23]. The samples were given a solution annealing treatment prior to irradiation. The irradiation conditions and the types of the materials are listed in Table 1. Bulk compositions for these six heats are presented in Table 2 as reported by Jenssen et al. from independent analyses on unirradiated samples. Although no systematic changes in composition are present in these heats, significant differences exist among the 304 and 316SS heats. Three low-carbon heats (304-C, 304-E and 316-F) are included with two intermediate carbon heats (304-B and 316-P) and one higher carbon heat 316-K. 304-E is a higher purity heat and contains lower levels of many elements such as Mo, Mn, Si, P and N than the other 304SS heats. Heat 316-F is a low-carbon heat with lower levels of Si and S compared to the 316-K and 316-P heats. Since major alloying elements are similar for Types 304SS heats C and E, some assessment of impurity composition on irradiation behavior may be possible even though the composition of many elements have changed among the heats. The 316SS heats show smaller differences among the three heats, limiting potential insights based on the bulk compositions and irradiation behavior.

Table 1
Dose conditions for the irradiated 304 and 316ss heats

ABB heat	Dose (n/cm^2, $E > 1$ MeV)	Dose (dpa)
304-B	0.8×10^{21}	0.7
	1.1×10^{21}	1.6
	3.4×10^{21}	5.0
304-C	0.4×10^{21}	0.6
	0.6×10^{21}	0.9
	3.4×10^{21}	5.0
304-E	0.8×10^{21}	1.2
	3.1×10^{21}	4.4
316-F	0.8×10^{21}	1.1
	3.3×10^{21}	4.7
316-P	0.8×10^{21}	1.1
	1.1×10^{21}	1.6
	2.0×10^{21}	2.9
	3.4×10^{21}	4.9
316-K	0.7×10^{21}	1.0
	1.1×10^{21}	1.6
	2.6×10^{21}	3.7
	4.0×10^{21}	5.7
	9.3×10^{21}	13.3

Thin slices were sectioned from the grip area of the irradiated and tested CERT specimens and 3-mm disks punched from the slices. The grip area experienced stresses well below the yield stress during testing, therefore the microstructure is considered to be unaffected by the testing. Specimen preparation involves electropolishing with a 5% perchloric/95% methanol electrolyte cooled to −40 °C using a polishing current of ~150 mA. A thorough characterization has been completed on each condition using weak-beam, centered dark-field, and high resolution imaging in a JEOL 2010F

Table 2
Bulk compositions of the solution annealed 304 and 316SS heats

	304SS			316SS		
	Heat B	Heat C	Heat E	Heat F	Heat K	Heat P
C	0.035	0.014	0.015	0.009	0.055	0.040
Cr	18.3	18.6	18.5	16.7	16.5	16.7
Ni	8.5	10.2	10.9	11.6	12.4	12.2
Mo	0.4	0.3	0.1	2.7	2.3	2.6
Mn	1.4	1.3	0.8	1.4	1.7	1.8
Si	0.65	0.43	0.05	0.26	0.64	0.59
P	0.031	0.023	0.006	0.021	0.016	0.024
S	0.029	0.006	0.009	0.001	0.006	0.007
B	<0.0004	<0.0004	<0.0004	0.0010	<0.0004	0.0013
N	0.067	0.077	0.039	0.062	0.029	0.058

FEG-TEM (field emission gun transmission electron microscope) and a JEOL 2000ES TEM. Defect sizes and densities were measured near the foil edge in regions less than 80 nm thick, which minimizes overlap of defects and improves the accuracy of the measurements. The defects were counted from digital images scanned from the original negatives. Thickness measurements were made using convergent beam electron diffraction, a standard technique with an error of ±5%. Compositional information was obtained in the 2010F using a Link EDS system with a probe size down to 0.7 nm.

As described in the introduction, Frank loops are faulted dislocation loops lying on the four {1 1 1} planes with a Burgers vector $a/3\{1\,1\,1\}$ and are clearly present in these irradiated samples at all doses. Examples of the diffracting conditions used to image the loops are shown in Fig. 1 for the 316SS Heat K at 1 and 5.6 dpa. The diffracting conditions are obtained by tilting ~8° away from the [0 1 1] zone axis along the $\mathbf{g} = 113$ reflection. At this imaging condition two edge-on variants will be visible while the other two are inclined. The relrods (encircled) are due to presence of the {1 1 1} stacking faults in the loops and can be used to image the Frank loops independent of the matrix. Depending on the exact orientation the relrods will be visible as either spots or streaks. Using the relrod allows the Frank loops to be measured to sizes less than 1 nm, although any feature much smaller than 1 nm begins to merge into a simple bright dot and becomes increasingly faint due to the smaller scattering area of the fault. Therefore, a practical lower limit of ~0.5 nm was found in this work based simply on the observation that Frank loops are hard to define as distinct edge-on loops below this size. For the lowest doses characterized in this study, the streaks in the diffraction pattern were not always visible due to the small average size of the loops; however, placing the aperture in the appropriate spot allowed the Frank loops to be imaged 'blindly'. The densities can be measured reliably from these images by taking into account the number of variants possible versus what is being imaged. Size distributions and density were measured from these images for each of the conditions examined.

A Nikon QM-1 high-temperature microhardness system and a Tukon Model 300 microhardness tester were used to evaluate the hardness of the various stainless steel samples using a load to 200 g. The temperature range examined in initial tests is 20–275 °C with intermediate test temperatures of 100 and 200 °C. Specimens were held at temperature for approximately 3 min before testing and a minimum of three indents were recorded. All specimens (typically 3-mm discs) were given a consistent metallographic surface preparation to a 6-μm finish using SiC paper.

Helium levels were checked for each irradiated material condition using an isotope-dilution mass spectrometry technique [24]. Helium contents were on the order of 10 appm at ~5 dpa for all of the heats except 316SS heats F and P, which contained slightly more boron. At ~5 dpa these latter two heats contained 20 appm helium.

3. Results

The results of the microstructural characterization will be presented first, describing the fine-scale defect microstructure produced during irradiation. Hardness results will also be presented for each dose and material condition to relate the microstructural changes due to irradiation to the measured changes in hardness.

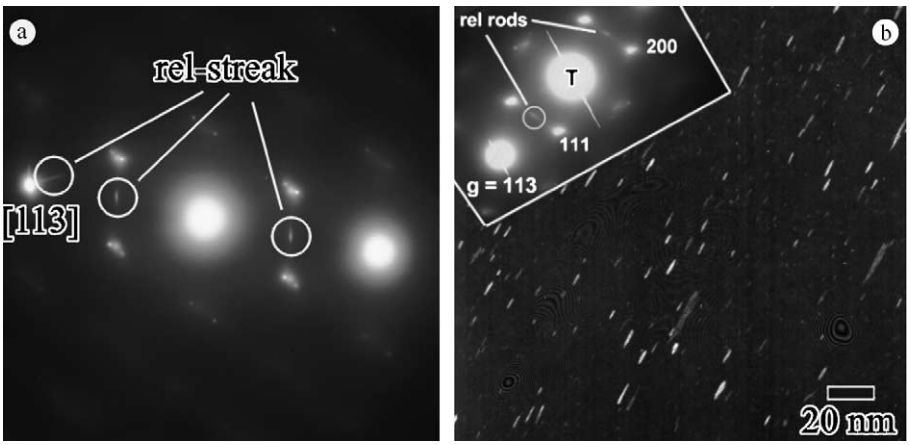

Fig. 1. Illustration of the imaging conditions used to image the small Frank loops in all 304 and 316SS heats. The reciprocal lattice streaks (encircled) are shown for (a) 1 dpa and (b) 5.7 dpa. The loop images in (b) show one variant of the loops when imaged using the encircled streak. Newton rings are present in the dark-field image and are simply artifacts of the image scanning.

3.1. Microstructural characterization

3.1.1. Unirradiated microstructures

The microstructure in each of the unirradiated materials is comprised of equiaxed grains with annealing twins present in approximately 40% of the grains. The grain size of the three 304SS heats is similar for all 3 heats, ranging from ~45 m for 304-C to ~60 m for 304-E. The 316SS heats exhibit a much larger spread in grain sizes with the 316-K at 50 μm, the 316-P at ~80 μm and the 316-F at ~150 μm. SEM examinations revealed a low density of Mn-S inclusions which are most common in the 304SS heats B and C. Examination of the unirradiated microstructures by TEM shows all six heats to be effectively solution annealed, with a low density ($<10^{12}$ m^{-2}) of isolated dislocations.

3.1.2. Identification of the fine-scale damage

The initial characterization of the irradiated material began with the lowest dose samples of 1 dpa or less. The microstructure in general appears to be free of any discernible dislocation network known to form at higher irradiation temperatures, and no cavities of any sort were observed in these materials. There was some indication of small precipitates on the order of 4–5 nm in size, but these were not present in a density of greater than $\sim 10^{20}$ m^{-3}. When imaged in bright field or matrix dark-field, the microstructures at these low doses are composed of a high density of very small defect clusters and small Frank loops. The small defects are difficult to resolve under these imaging conditions and lend themselves well to the generic description of 'black dots' in the bright field images. At the low doses, only a fraction of the defects can be easily distinguished as Frank loops, most of which are more than a few nanometers in diameter. However, by imaging the defects using the relrod technique described earlier, the small hard-to-resolve defects are found to be simply small Frank loops. The black dots are therefore a combination of edge-on Frank loops that are more easily distinguishable at larger sizes and the inclined variants that appear as small round defects.

The example in Fig. 2 show more clearly the appearance of the Frank loops in the 316-K at various doses. The images compare the appearance of the loops in matrix dark-field with the centered dark-field images obtained using the relrods from the faulted loops. The dark-field images shown in Fig. 2(b) and (d) were taken on a $\mathbf{g} = 200$, 2-beam condition, which shows all four of the Frank loop variants, two edge-on and the two inclined variants, the latter of which are not very clearly defined at these small sizes. Measuring the size of the defects reliably from these dark-field images is difficult because of the overlap between defects and their interacting strain fields, particularly when the foil thickness is much larger than 80–100 nm and the size begins to exceed an average of a few nanometers. The weak-beam image shown in Fig. 2(f) illustrates the difficulty in accurately characterizing the defect microstructure under these imaging conditions. By comparison, the centered dark-field images shown in Fig. 2(a), (c) and (e) obtained by using the relrods shown in Fig. 1 enable a more accurate measurement of the Frank loops.

The strain field images of the loops, that is, the images taken in bright field or matrix dark-field, do provide useful information, however. Other types of defect structures such as SFT and prismatic dislocation loops ($\mathbf{b} = a/2\langle 1\,1\,0\rangle$) can form directly from the cascade collapse and subsequent interaction between the point defects and their clusters, as well as unfaulting of the Frank loops. To evaluate the possibility that there may be another component of the microstructure present such as SFT or prismatic loops, samples were imaged in two different 2-beam conditions ($\mathbf{g} = 200$ and 113) near the same zone [0 1 1] axis. These images were taken from two doses in 316-K and 304-B at ~1 and 5 dpa to cover an appropriate dose range. At the $\mathbf{g} = 200$ orientation, all four of the Frank loop variants, 2/3 of the possible six prismatic variants and all of the SFT should be visible. The densities measured from these pictures fall within the scatter of the overall density data obtained from the relrod images, indicating that no additional microstructural features are present in any significant density. The same was found for those images taken using the $\mathbf{g} = 113$ condition where 3/4 of the Frank loops variants are visible and 5/6 of the possible prismatic variants should be visible if present. While this does not conclusively prove that no unfaulting occurs or that other types of defects are present besides small Frank loops, it does further strengthen the argument that only small Frank loops form in significant density under the irradiation doses and temperatures examined in this study.

There are triangular-shaped images that appear in the irradiated stainless steels, however, that can be confused with SFT. Several cases have been observed in these materials where small, triangular-appearing defects appear in the matrix dark-field and bright field images when taken near a dynamical 2-beam, $\mathbf{g} = 200$ condition. Examples of these triangular defects are encircled in the images shown in Fig. 3. While these triangular-shaped defects appear to be SFT, imaging the same defects by lattice imaging clearly show that these are simply small Frank loops lying on edge. The triangular appearance of many of the defects shown in Fig. 3 is thought to be due to the asymmetric strain field contrast of the small defects that varies significantly depending on the diffracting condition and position relative to the foil surface. Changing the diffraction condition by moving the diffracted spot around inside the objective aperture alters the appearance of the strain field, in some cases shifting the triangular strain contrast to the other side of the edge-on loop or eliminating it

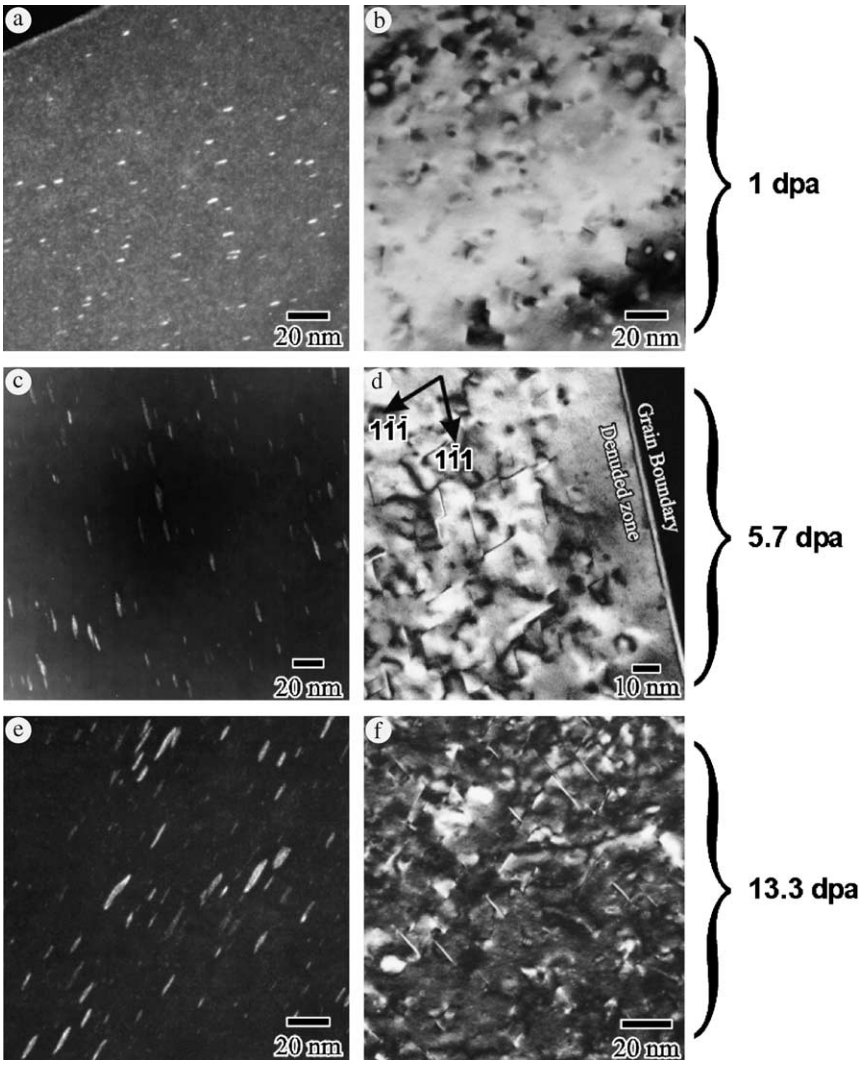

Fig. 2. The Frank loop microstructure is shown for various neutron doses in the 316SS heat K. The Frank loops in (a) and (b) are from the 1 dpa condition, the loops shown in (c) and (d) are from the 5.7 dpa condition, and (e) and (d) are from the 13.3 dpa condition. The matrix dark-field images shown in (b), (d) and (f) illustrate the complex images obtained when imaging the strain fields in the matrix from the high density of loops. The loops in the three relrod dark-field images provide a clearer idea of the size and density.

altogether. Note that in many cases the rel-rod images of the Frank loops are ellipses when they are inclined to the beam direction, indicating that they are more or less circular loops.

Evidence of SFT and intermediate defect configurations were found in limited cases as illustrated by the lattice images provided in Fig. 4. Fig. 4(a) reveals two widely separated Frank loops in 316-K at 1 dpa with no evidence of another bounding Frank partial as would be expected in an SFT. Fig. 4(b) gives two examples in 304-E at 1.2 dpa where the triangular-shaped defects are possibly partially-dissociated Frank loops following the examples provided by Jenkins and Kirk [25]. An SFT should have equal lengths for two straight interfaces if fully contained within the foil, however, the disparity in their lengths suggest that this may actually be a partially-dissociated Frank loop. Jenkins and Kirk have given examples of the types of contrast that can arise from partially-dissociated Frank loops in both pure copper and silver, and those images are similar to those presented here. The partially-dissociated Frank loops represent a situation where the defect structure is intermediate between a Frank loop and an SFT. Jenkins and Kirk pointed out that the partially-dissociated Frank loops can be mistaken for either complete SFT or even as multiple Frank loops depending on the imaging conditions. This problem will simply be exacerbated in situations where the density and size leads to image

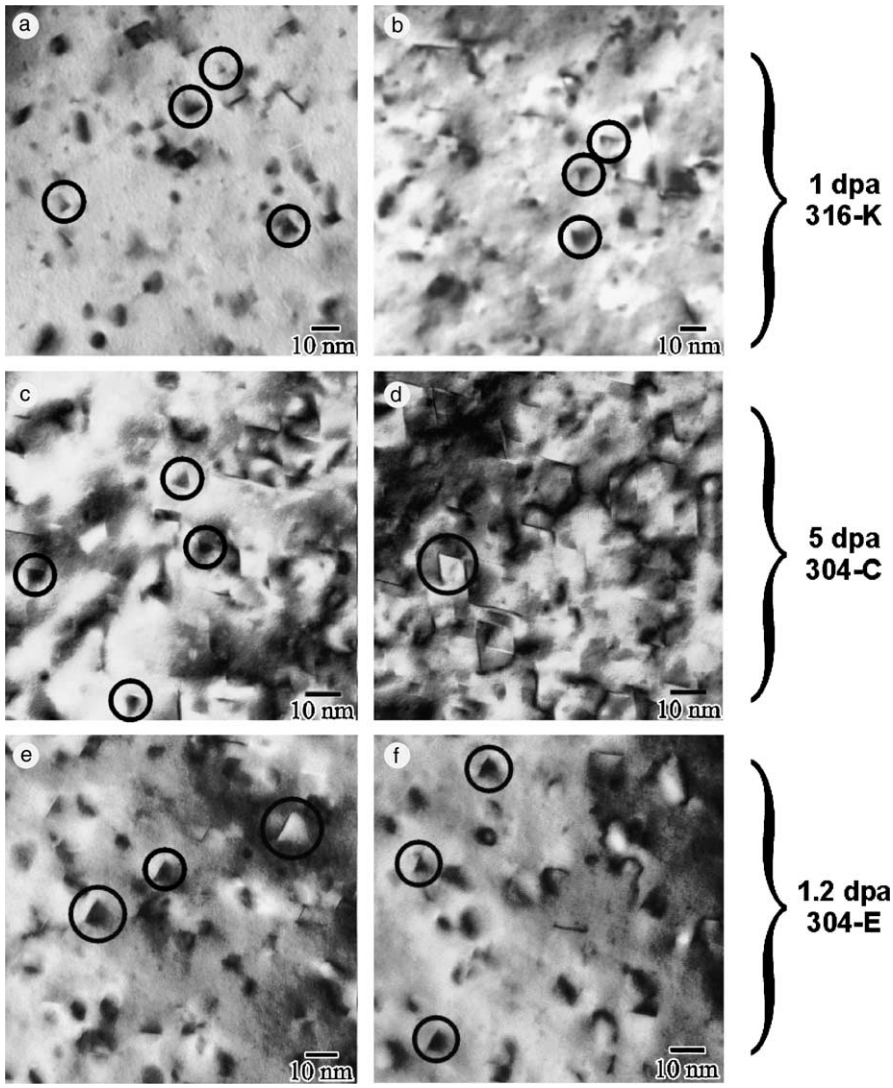

Fig. 3. Triangular-shaped strain fields can be mistaken for stacking fault tetrahedra. The examples shown here are from images taken near a $\langle 0\,1\,1\rangle$ zone axis under a $\mathbf{g} = 200$, 2-beam dark field condition. The defects in (a) and (b) are from heat K at 1 dpa, the defects in (c) and (d) are from heat C at 5.0 dpa, and the defects in (e) and (f) are from heat E at 1.2 dpa. In many cases, the triangular appearance is the result of an asymmetric strain field from a single Frank loop.

overlap of the Frank loops. Evidence of SFT do exist in the low dose 304-E as shown Fig. 4(c)–(f). Comparing the matrix dark-field and lattice images of the two individual SFT shows quite clearly that there are two interfaces of equal length present on each defect, unlike the single fault shown in Fig. 4(a) for the Frank loop.

In all of the commercial 304 and 316SS (heats B, C and P and K, respectively) and for the somewhat higher purity 316-F, no consistent evidence of SFT are found. For the highest purity 304-E, a small fraction of the defects are found to be SFT based on weak-beam images and the lattice images, examples of which are shown in Fig. 4. The number of SFT are estimated to comprise less than 5% of the observed defects, and their distribution is not homogenous. Some areas contain several SFT while others are completely devoid of any defect type other than Frank loops.

3.1.3. Characteristics of the Frank loops

Having determined that the visible microstructure is composed of predominately Frank loops, images were taken for each dose and each material to compare the Frank loop microstructure. Densities and sizes were measured from images taken using the rel-rods to image one variant of the Frank loops at a $\mathbf{g} = 113$, 2-beam condition as described above. All images were taken at

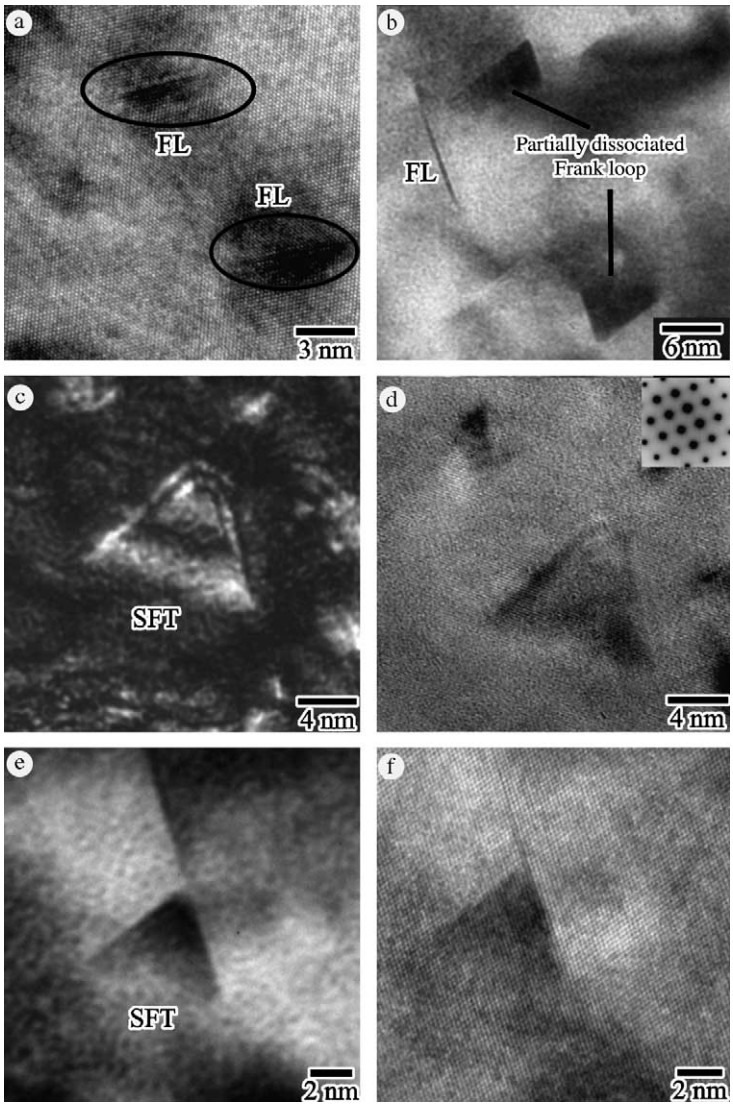

Fig. 4. Lattice images from defects in different irradiation conditions are shown. All images were obtained from a foil tilted onto a $\langle 0\,1\,1\rangle$ zone axis. The defects in (a) are single Frank loops in 316SS heat K at 1 dpa. The remaining images are from the higher purity 304SS heat E at 1.2 dpa. The defects shown in (b) are thought to possibly be partially-dissociated Frank loops, whereas the complementary matrix dark-field/lattice images shown in the sets (c)/(d) and (e)/(f) are thought to be SFT.

magnifications of 150 000× or above, and analyzed digitally from scanned photos.

The Frank loop size distributions for all six heats (using a common bin size of 1 nm) are shown in Fig. 5, and the density and average size as a function of dose are provided in Fig. 6 and listed in Table 3. A comparison of the size distributions at two doses is given in Fig. 7. The size distributions in Fig. 5 show that the Frank loop evolution is relatively consistent between the two heats 304-B and 304-C and the two heats 316-K and 316-P despite their different compositions. Size distributions for the lowest doses tend to be narrow, Gaussian distributions that eventually broaden at higher doses into a somewhat asymmetric distribution that extends up to ~30 nm. The narrow size distributions at the two lowest doses in the 304-B and 304-C illustrate that most of the loops are in the regime traditionally ascribed to the black spots. As the dose increases the loops appear to grow and therefore shift the average sizes upward. An effective saturation state is reached for all of the heats above ~3 dpa. The size distributions for the 304-E and 316-F reveal a somewhat different trend. At 1 dpa, they are broader than for the other four heats, particularly with regard to the 304-E, and this trend holds true at the

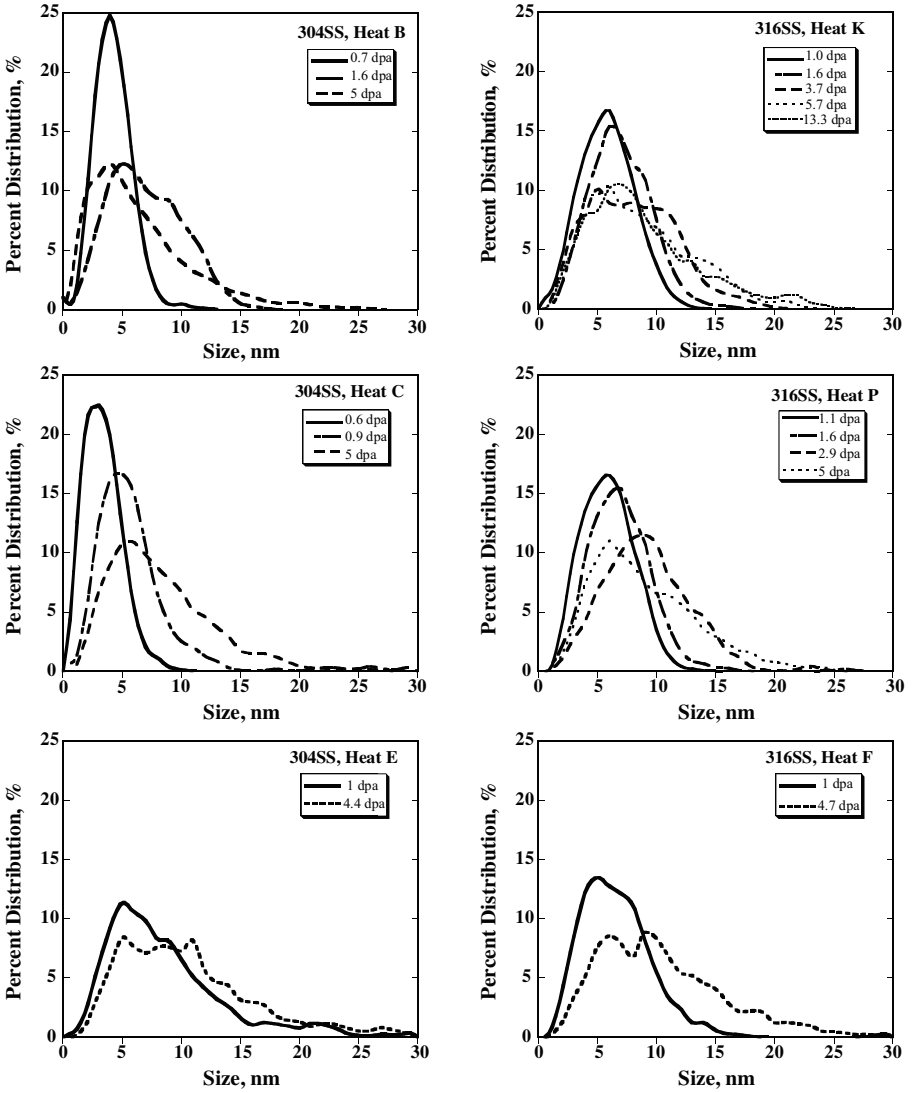

Fig. 5. Frank loop size distributions are provided for all of the various conditions and materials characterized in this experiment. Most size distributions at 1 dpa or less in heat K, P, C and B are narrow Gaussian profiles that broaden as the dose increases above 1 dpa. The size distributions for the two higher purity heat E and F are broader than their commercial purity counterparts at 1 dpa, indicating that the loops evolve faster. Above a few dpa all size distributions are asymmetric and in some cases a second peak may be appearing.

higher dose. For the bin size chosen to make these size distributions, a second peak appears at the highest dose in both materials, but whether this is statistically significant or is an artifact due to the choice of bin size is unclear. The broader size distributions at lower doses and the appearance of a possible second peak at 5 dpa suggest that the higher purity heats evolve at a moderately faster rate than their more lower purity counterparts.

The densities measured for the individual heats reveal that with the exception of 304-B, the loop density in most heats is already established at near saturation levels by 0.6–1 dpa. There are some minor differences between the different heats, especially for the heat C which possesses a lower saturation density than the other five heats. The density of loops in 304-B is higher than the other heats at 5 dpa, but no data is available past 5 dpa to determine whether the density will continue to increase or saturate as in the other heats. The average density for all of the heats lies around 2×10^{23} m^{-3} for 1 dpa and higher doses except for the two cases just cited. The most noticeable changes therefore are the increases in average size due to the broadening size distributions. At a dose of $\sim$1 dpa, the average sizes of

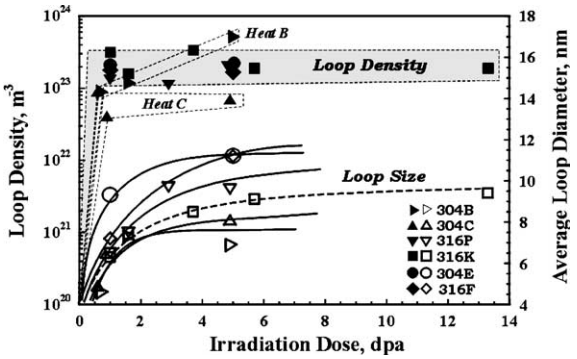

Fig. 6. The average size and density of the loops in the various materials are presented here. Density of loops is established by ~1 dpa if not sooner, and most heats exhibit a saturation density around $\sim 2 \times 10^{23}$ m^{-3}. Heat C and B show some differences in density compared to the other heats. The loops sizes increase with dose in all heats, but this increase begins to taper off fairly quickly above 2 dpa. The two higher purity heats E and F possess larger Frank loops on average than the less pure heats.

Table 3
Average size and density of Frank loops in the irradiated 304 and 316SS heats

ABB heat	Dose (dpa)	Loop density ($\times 10^{23}$ m^{-3})	Mean size (nm)	$(Nd)^{1/2}$ ($\times 10^{7}$ m^{-2})
304-B	0.7	0.9	4.6	2.0
	1.6	1.2	7.3	3.0
	5.0	5.2	6.9	6.0
304-C	0.6	0.9	4.9	2.1
	0.9	0.4	6.5	1.6
	5.0	0.7	8.1	2.4
304-E	1.2	2.1	9.3	4.4
	4.4	2.5	11.2	5.3
316-F	1.1	1.8	7.2	3.6
	4.7	1.7	11.2	4.4
316-P	1.1	1.3	6.4	2.9
	1.6	1.6	7.5	3.5
	2.9	1.1	9.7	3.3
	4.9	2.0	9.6	4.4
316-K	1.0	3.2	6.3	4.5
	1.6	1.6	7.4	3.4
	3.7	3.4	8.5	5.4
	5.7	1.9	9.1	4.2
	13.3	1.9	9.4	4.2

the Frank loops for most of the heats are around 7 nm, with the average size significantly higher in the 304-E. As the dose increases the differences between the individual heats become more discernible such that at 5 dpa the average sizes range from ~7 nm for the heat B to ~11 nm for both 304-E and 316-F. The data for 316-K suggests that changes beyond a few dpa are relatively small once saturation is achieved.

3.1.4. Near grain boundary regions

Irradiation also led to changes in the near-boundary regions in the form of defect-denuded zones as illustrated in Fig. 8. The measured width of these denuded zones is plotted in Fig. 9, showing that the denuded zones disappear after a few dpa. The biggest surprise is not the presence of the denuded zones however, but rather that there is a noticeable and consistent difference in the width of the zones in the 304SS alloys versus the 316SS alloys. In addition, the denuded zones are thought to disappear much earlier in the case of the 304-B and 304-C than in 316-K and 316-P. However, since no data exists for the doses between ~6 and 13.3 dpa, it is not possible to say exactly at what dose the denuded zones disappear for the 316SS. No denuded zones were found in either the 304-E or the 316-F, which tends to support the observation made earlier that these two alloys evolved at a faster rate than the other four heats.

In addition to the denuded zones, RIS alters the chemical composition of the grain boundaries and near-boundary regions, although the scale is considerably smaller than the width of the denuded zones. These results have been summarized earlier by Bruemmer et al. [26] and will not be presented in detail here. They showed that Ni and Si can enrich at the grain boundaries to levels of 30 wt% and 8%, respectively, which is accompanied by the depletion of Cr and Fe. This represents a substantial change since the matrix levels in 316SS are around 12% Ni and 0.5% Si. The widths of these profiles are approximately ±5 nm, although they there are some minor changes that continue out to ±10 nm. The changes in composition are not limited to just the grain boundaries since Ni and Si are found to be enriched at the Frank loops in the 316-K irradiated to ~13 dpa. The larger loops and higher levels of RIS present at this dose allow the enrichment to be measured by EDS on a few of the larger edge-on Frank loops. This latter result is not quantitative because only a few loops were examined, no profiles were taken across the edge-on loop, and the concentrations are diluted to some extent since the loops are buried within the foil. The degree of segregation to the loops needs to be further investigated as a function of loop size.

3.2. Hardness results

Hot hardness tests were performed on all of the heats investigated in this study, with a summary of the data given in Table 4. Fig. 10 compares the dose dependence of the hardness of the 304 and 316SS heats at 275 °C. A substantial amount of the hardening occurs already at doses of less than 1 dpa, the dose regime where most of the defects are less than 10 nm in diameter. In general

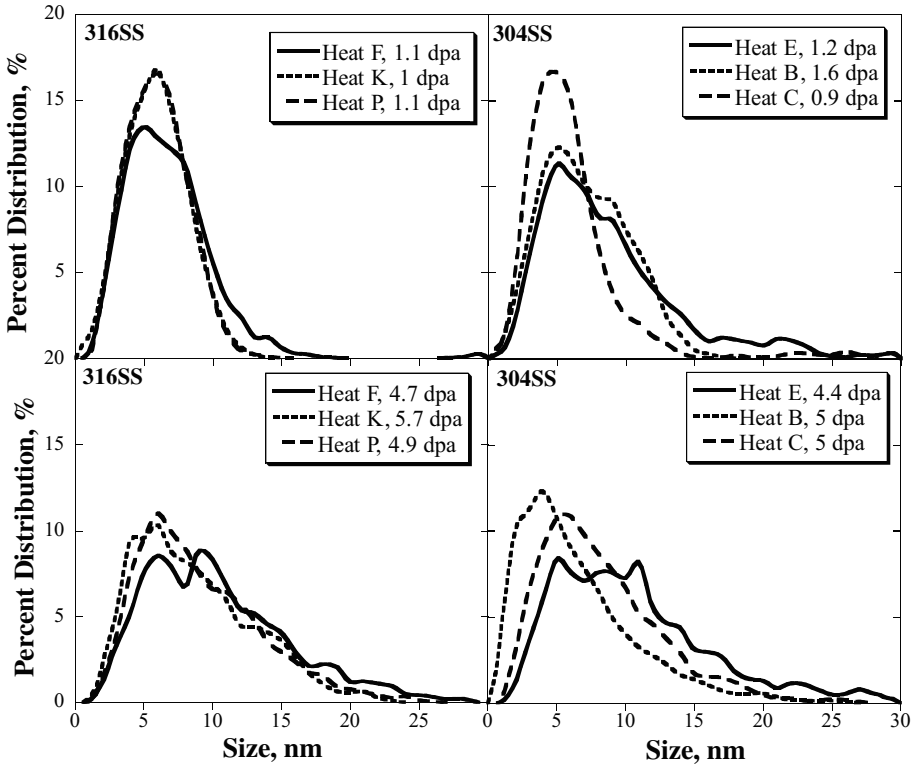

Fig. 7. A comparison of the size distributions for two different doses shows more clearly both the similarities between the less pure heats K, P, B and C and the more rapid evolution of the loops in higher purity heats E and F. The differences at 1 dpa are not so noticeable, but by ~5 dpa the loop distribution in heats E and F has broadened more, with a second peak appearing.

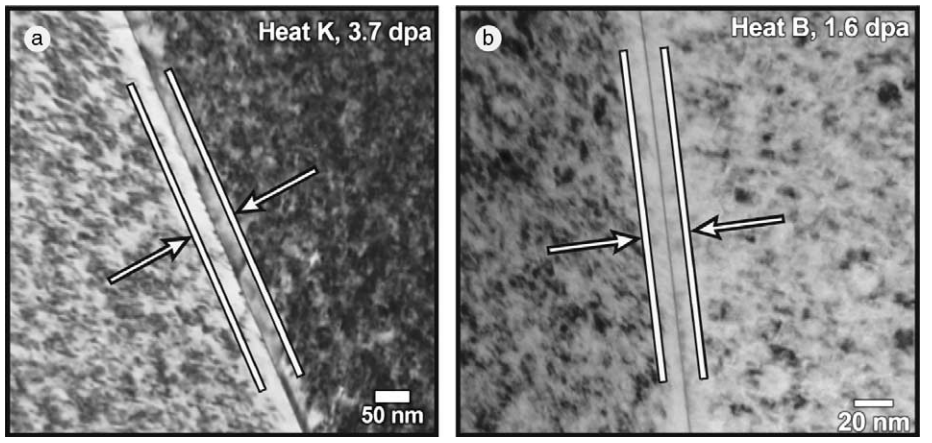

Fig. 8. Denuded zones were found in all of the heats except for the higher purity heats E and F. The denuded zones appear to form at lower doses, but as shown in the next figure, they disappear at higher doses. The width of the denuded zones is substantially lower in the 304SS compared to the 316SS.

the heats 304-B, 316-K, and 316-P behave the same at doses less than a ~2 dpa, but at 5 dpa heat 304-B hardens to a higher level than the other two heats. Heats 304-C, 304-E and 316-F are consistently lower in hardness than the heats B, K and P. Fig. 11 compares the temperature dependence of the hardness for two different doses. Increasing the test temperature lowers the hardness values for all of the heats, but maintains the

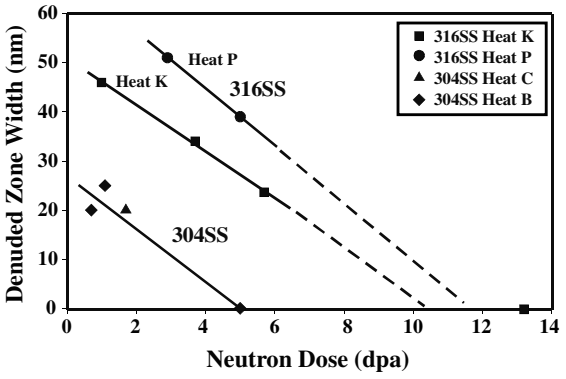

Fig. 9. The denuded zones in the 304SS heats C and B were approximately half the width of the loops in the 316SS. No denuded zones were found in the 304SS at 5 dpa, whereas they still persist in the 316SS. It is not known precisely at what dose the denuded zones disappear in the 316SS, but eventually the loops nucleate and grow up to the boundary.

Table 4
Average hot hardness results for 304 and 316SS heats (kg/mm^2)

ABB heat	Dose (dpa)	Test temperature (°C)				
		20	100	150	200	275
304-B	0	149		98		86
	0.7	278	249		234	220
	1.6	331	306		266	250
	5.0	460	390		355	343
304-C	0	155		105		92
	0.9	265	206		170	147
	1.7	290	232		199	165
	5.0	356	321		288	255
304-E	0	130		105		92
	1.2	258	232			183
	4.4	303	275			207
316-K	0	161		133		101
	1.0	307	276		248	218
	1.6	282	268		243	234
	3.7	342	309		278	265
	5.7	419	344		320	311
316-P	0	161		133		101
	1.1	277	249		234	220
	1.6	297	264		256	238
	4.9	331	301		286	260
316-F	0	161		133		101
	1.1	219	195			170
	4.7	282	255			227

overall differences between the different dose levels. For both dose conditions the heat B material is harder for all the test temperatures. At ~1 dpa, the 316-F displays the lowest hardness, followed closely by the 304-C and then the 304-E. At ~5 dpa, the data show that both the higher purity heats E and F are lowest in hardness, whereas the heat C is more comparable to the 316SS heats P and K.

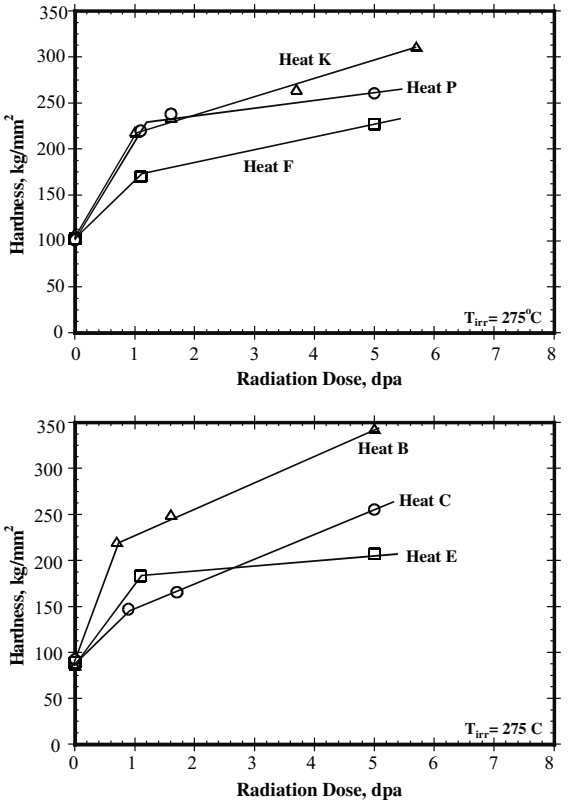

Fig. 10. The dose dependence of the hardness at 275 °C is shown for each of the six heats. All of the materials exhibit considerable hardening below 1 dpa in the regime where the defects are typically referred to as black dots. As the dose increases, all heats continue to increase in hardness but to different degrees.

4. Discussion

As outlined in the results section, the rel-rod technique employed in this study clearly shows that the Frank loops extend down into the size range usually attributed to black spots. This has important repercussions in regard to understanding the overall evolution of the vacancy and interstitial components of the microstructure and how this relates to mechanical properties. In particular, the hardness results demonstrate that a substantial amount of hardening occurs before 1 dpa, which means that the very small defects, in this case Frank loops, play an important role in the hardening behavior.

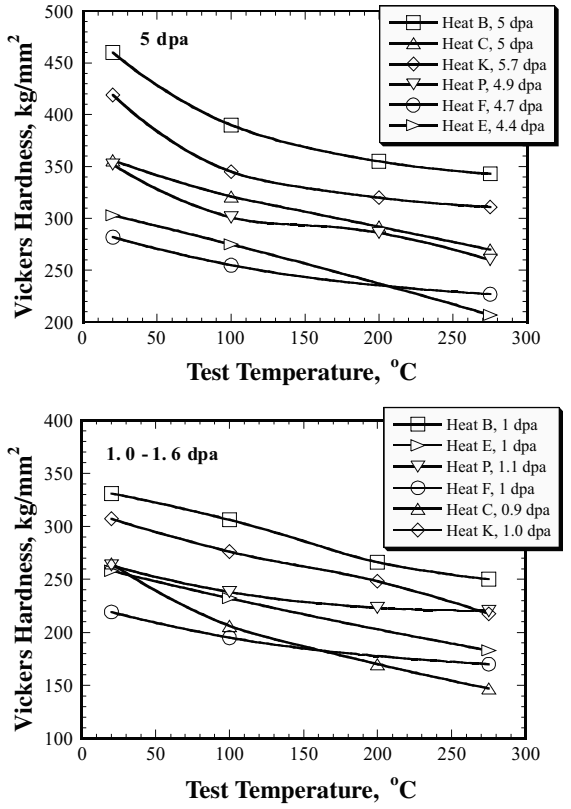

Fig. 11. The hardness decreases for all of the heats as the test temperature increases. Surprisingly, the two higher purity heats E and F are lower in strength than the other heats at 5 dpa. At lower doses the differences are not so noticeable. The 304SS heat B is consistently the harder materials at all temperatures and doses.

4.1. Microstructure evolution – Frank loop versus black spots

The results presented show that the Frank loops dominate the microstructure as early as 0.6 dpa, the lowest dose characterized in this study. The density reaches a saturation level for most of the heats at ~1 dpa, but this level varies from heat to heat and is lowest for the 304-C. The size distributions continue to change gradually as the dose increases, but the rates of these changes appear to slow above ~3 dpa. In many of the previous studies and reviews where the authors partitioned the defect microstructure into two components, black spots and Frank loops, combining the densities of the two separate components they reported yields a density similar to that observed for the Frank loops characterized in this study. As an example, Maziasz [1] placed the density of black spots at around 3×10^{23} m^{-3} and the Frank loop density at around 1×10^{23} m^{-3}. Combining these separate densities yields a total density of defects at saturation at about 4×10^{23} m^{-3}, slightly higher than the average density measured in this study, but well within the scatter of the data presented here. Lee et al. [10,11] recently conducted a study on 316LN irradiated with 360 keV He ions at 200 °C. They found a mixture of small defects (black spots) assumed to be a mixture of vacancy-type SFT and small interstitial loops, intermixed with larger defects (>5 nm) they considered separately as Frank loops. The densities of Frank loops and black spots were on the order of $2–4 \times 10^{23}$ m^{-3} when added together.

Bailat et al. [16,17] characterized four stainless steel heats (one commercial purity variant of 304L and 316L each, and one high-purity variant of 304L and 316L each) that were neutron-irradiated to 1.5 and 7.5 dpa at 275 °C in the Barsebäck reactor. They found that in both of the 316SS heats and the HP304 heat the density of loops at 7.5 dpa was $\sim 1.7 \times 10^{23}$ m^{-3} with an average size of 6.0–7.5 nm depending on the heat. The CP304 heat had a slightly higher density of 3×10^{23} m^{-3} with an average size of 7.3 nm. The average sizes of these loops are well within the range cited in this study for all of the defects measured in the different materials at comparable doses. They also performed 590 MeV proton-irradiations to 0.15 dpa at ~250 °C on the unirradiated materials to compare the microstructures with the neutron case. At this dose, they were able to only positively identify about 30% of the visible defects as Frank loops with an average size of 2–3 nm, the rest they referred to as 'black dot' damage. Interestingly enough, in the low dose proton-irradiated samples the total density of defects (black spots and Frank loops) in the CP304 heat was $\sim 3 \times 10^{23}$ m^{-3} whereas for the 316SS heat P the density was only $\sim 3 \times 10^{22}$ m^{-3}, considerably lower. No systematic attempt was made to ascertain the true defect nature for the larger loops they measured or the smaller defect clusters.

In summary, the densities presented by different authors tend to agree with the results presented in this study when defect densities are added together, that is, the black spots and Frank loops are considered to be all Frank loops. None of these studies, as in the present case, have been able to elucidate directly whether the small Frank loops are indeed only interstitial-type loops Frank loops or include vacancy-type Frank loops. In the following paragraphs we will make a case for the small Frank loops being of both types for a number of indirect reasons.

4.2. Microstructure evolution – vacancy versus interstitial-type Frank loops

In many of the earlier irradiation studies the nature of the black spot damage and even the small Frank loops was not fully characterized. The idea that all Frank loops are interstitial in nature seems to have

arisen because of an extrapolation of results obtained from higher irradiation temperatures. The breeder reactor studies conducted in the 1970s on stainless steels involved irradiations at temperatures greater than 400 °C (and usually doses of >10 dpa), which produces a complex mixture of Frank loops, voids, bubbles and precipitates. Frank loops produced under these conditions are often 20–200 nm in size and have been identified as interstitial Frank loops by different researchers [5–8]. The vacancy component of the radiation damage likely resides in the visible voids that formed under these irradiation conditions. Note that above 300 °C the stability of vacancy-type defects changes such that small vacancy loops are likely to be thermally unstable and emit vacancies into the lattice, allowing gas-stabilized cavities to form [2]. Interstitial loops remain stable up to much higher temperatures, presumably due to the difficulty in removing interstitials from the loops, preferential absorption of interstitials ('dislocation bias') and the presence of more stable vacancy-type sinks such as gas bubbles and voids.

In a recent study on the deformation microstructures and mechanisms in irradiated austenitic stainless steels, Lee et al. [27,28] state that all Frank loops observed in irradiated austenitic stainless steels are interstitial in nature, and that large vacancy-type Frank loops cannot grow to large sizes because they will unfault. They do not, however, provide an estimate of this limiting size. This view that low-temperature irradiated stainless steels contain interstitial-type Frank loops only and that the vacancies are tied up in the remaining black spot damage distinct from the Frank loops still prevails in many recent studies. While this study cannot confirm directly the nature of the Frank loops less than 10 nm in size, it seems likely based on the argument of equal production of vacancies and interstitials that the resolved defects are composed of both vacancy and interstitial-type Frank loops. The assumption that the Frank loops are strictly interstitial in nature is dubious given that this assumption is extrapolated from a much higher irradiation temperature where (a) the Frank loops are much larger (>50 nm) and therefore more easily characterized, and (2) voids are often present to account for the vacancy component of the radiation damage.

The previous reviews by Maziasz [1], Zinkle et al. [2], and Bruemmer et al. [3] postulated that the black spot damage forms directly in the cascade process as small vacancy clusters. The present results suggest that small Frank loops may indeed form directly from the cascade, but are likely to be both interstitial and vacancy-type. Dislocation theory treats the formation of Frank loops due to the condensation of vacancies or interstitials on the {1 1 1} planes [29], so there is certainly a theoretical basis for the formation of both types of loops. In the case of pure metals such as copper and nickel, the SFT that form are considered to have formed primarily from the cascade collapse and yield a narrow size distribution that peaks around 2–3 nm and is relatively independent of dose up to 0.3 dpa. In the stainless steels irradiated in this study, the narrow size distribution of the loops at doses less than 1 dpa are in a similar size range, suggesting that the loops may have formed directly from the cascade. However, one cannot eliminate the possibility that some fraction of the loops formed during irradiation nucleate independent of the cascade process and then grow by absorption of point defects. Regardless of how the loops are formed, the increase in average size and the broadening of the size distributions with increasing dose indicates that loop growth continues up to high doses.

The size distributions often show or at least hint of a secondary peak at higher doses (for the common bin sizes chosen for these plots), which may reflect that one component of the microstructure, perhaps the interstitial Frank loops, are growing faster than the other. The second peak is more prominent at ~5 dpa in the 304-E and 316-F, both of which contain lower concentrations of minor elements than the other four heats. This preferential growth of the interstitial loops, if it in fact exists, may arise from several sources. First, the high formation energy of interstitials, on the order of 2–4 eV for interstitials [30] compared with the 1.5–1.9 eV for vacancies [31,32], means that shrinkage of the interstitial-type loop likely occurs by vacancy absorption only, whereas the vacancy-type loops could shrink by the emission of vacancies into the lattice and absorption of interstitials. RIS of nickel and silicon, and potentially other elements such as carbon, could affect the stability of the loops, however, the mechanism by which this segregation influences defect behavior is unknown at this time. A further issue to consider is if the vacancy-type Frank loops are unable to grow to large sizes because it is either energetically unfavorable or they unfault, then this may shift the balance in favor of the interstitial-type Frank loops.

The observation that SFT are found only in the higher purity 304-E raises an important issue concerning minor elements. In light of the present work, the presence of carbon, silicon and phosphorous as well as other impurities/additions may alter the evolution and types of defects that form during irradiation. These minor elements may alter the diffusion of vacancies and interstitials by solute binding, and their segregation to defect complexes could alter the stability of Frank loops versus SFT. Zinkle et al. [2] postulated that this explained why so few SFT are present in commercial purity stainless steels when compared to the pure metals such as copper and nickel, where SFT comprise a large percentage of the fine-scale defect population.

Note that in the often-cited work of Horiki and Kiritani [9], the material characterized in their study was a ternary Fe–15Cr–16Ni alloy made by melting the pure

elements together, considerably cleaner than the alloys examined in this study. They also irradiated the material at 200 °C to 0.14 dpa, much lower than the doses reported in this work. They reported finding that SFT were the dominant defect type at a density of $\sim 2.1 \times 10^{23}$ m^{-3}, whereas the interstitial loops were reported at a lower density of 2.2×10^{22} m^{-3}. The size distributions they reported indicated that both types of defects at this dose level were in the 2–4 nm average size range. Given the different irradiation conditions in their study and the higher purity of their materials, it seems questionable to assume that their microstructural state represents that of more highly irradiated stainless steels.

Some of the triangular-shaped defects observed in this study exhibit the appearance of partially-dissociated Frank loops, which according to Jenkins and Kirk [25] represent an intermediate configuration between an SFT and a Frank loop. While interstitial-type SFT are theoretically possible, no evidence has ever been found for their existence in any material and subsequently SFT are considered to always be vacancy in nature. In this case, the partially-dissociated Frank loops may represent vacancy-type defects that are unable to complete the transition from a Frank loop to an SFT. According to Hirth and Lothe [29], an SFT can form by extending a Frank loop by the condensation of vacancies, leading to a dissociation reaction along the edges of the Frank loop aligned along the $\langle 1\,1\,0 \rangle$ directions. This mechanism suggests that locally altering the stacking fault energy by solute segregation could influence the transformation since the extension of the Frank loop involves a dissociation reaction. Likewise, solute pinning could occur that would prevent the transformation from reaching its conclusion. The presence of these partially-dissociated Frank loops again is indirect evidence that character of the Frank loops may not be strictly interstitial.

Another possibility that needs to be considered with respect to the location of the vacancies is that small clusters of vacancies (and interstitials also) may be present that are too small to be imaged distinctly from the Frank loop microstructure. There is only limited evidence in the literature to support this hypothesis at this time, mainly derived from positron annihilation studies in a 316SS irradiated at 60 °C to $\sim 10^{-4}$ and 10^{-5} dpa with 14 MeV neutrons. Fukushima and Shimomura [33] found that a high density of small three-dimensional clusters of vacancies must be present to account for their results, and that the clusters may include only 2–3 vacancies. The temperature and dose conditions in their experiment are far removed from the conditions considered in this study, however. Given that clusters this small cannot be imaged easily in the TEM for quantitative data, it is difficult to speculate if these types of clusters exist in the materials characterized in this study and what their concentrations would be under these conditions. The size and density of the visible Frank loops present after a few dpa leave little volume that is unaffected by the strain fields of the visible loops. This level of microstructural saturation produces a highly strained lattice, making it seem unlikely that a high density of submicroscopic clusters can survive intact without being attracted to the nearby visible loops. Further, if the vacancies are contained in small, sub-nanometer clusters mostly invisible in the conventional TEM, the argument of equal production of vacancies and interstitials would imply a very high concentration of vacancy clusters ($>10^{24}$ m^{-3}) to balance the supposed interstitial-only Frank loops. This seems implausible to the authors since such densities of small clusters superimposed over the already high density of much larger Frank loops would mean most defects are touching each other, or are close to touching.

4.3. Relationship between hardness and microstructure evolution

One of the complications in relating the microstructural evolution and hardening behavior in the irradiated stainless steels evaluated within this study is that significant variations exist in the minor element content, namely, C, Si, P, N and S. Miwa et al. [34] and Tsukada et al. [35] attempted to study the influence of individual additions of C, Si, S, P and Ti on the properties of high-purity 304 and 316SS irradiated at 240 °C to ~1 dpa. They concluded that C (0.60–0.98 wt%) increases the density of Frank loops and significantly alters the tensile response of the material compared to the ternary Fe-CrNi material. Adding Si (0.65 wt%) suppressed the density of Frank loops, lowered the observed hardening and increased the work hardening and elongation compared to the base material. S, Ti and P had little effect on the microstructural evolution and hardening. When they added all of the elements into the alloy, the tensile behavior resembled that of commercial purity heats, indicating a complex interaction between the available solutes and defects produced during irradiation. Based on their observations, one can conclude that simple additions of C and Si can have opposite effects on the microstructural evolution and resulting mechanical properties, but added together or with other minor elements or impurities their impact is minimized.

Unfortunately, a comparison between their data and the data presented here is not possible for two reasons. First, their reported densities of loops (and black spots when given) are generally lower by a factor of 3–4, possibly a consequence of imaging the loops in bright/dark-field in regions thick enough to cause problems with overlap of loops. Secondly, in this study, the alloys all contain a number of alloying elements or impurities in varying levels, including C, Si, N, P and S. Because of

this, the effect of the individual elements cannot be evaluated separately except in the broadest sense. In this respect, the higher purity heats 304-E and 316-F are notable in that they possess the largest average size of loops and broader size distribution for a given dose, presumably because their loop microstructure evolves more quickly than the lower purity heats. However, despite having a larger average size, broader size distribution and comparable density of Frank loops, the hardness data (Table 4, Figs. 10 and 11) shows quite clearly that these two heats are consistently lower in hardness than their respective counterparts. The implications of this are briefly explored in the following analysis.

The relationship between the microstructure and the hardness can be made by comparing the change in hardness versus the parameter $(Nd)^{1/2}$ where N and d represent the number density and average size of the obstacles, in this case Frank loops. Note that unlike the previous studies mentioned throughout, only Frank loops will be included in this analysis, that is, there is no need to use superposition laws to add in the contributions from Frank loops and black spots. This parameter $(Nd)^{1/2}$ is derived from the dispersed barrier hardening model [36], which relates strengthening by a dispersion of obstacles in materials by the following relationship:

$$\Delta\sigma_{\text{yield}} \propto (Nd)^{1/2}.$$

For the purposes of this brief comparison the change in hardness will be used to represent the change in yield since they are nominally proportional to each other. Fig. 12 shows that when comparing the data for all of the heats at a particular dose, the 'effective' strength of the Frank loops has to vary between different heats to account for differences in hardening for a given size distribution and density of Frank loops. The clearest example of this behavior is in the three different 316SS heats, where together they have the same $(Nd)^{1/2}$ value, but obviously exhibit different levels of hardening at each of the two doses shown in Fig. 12. Comparing the 304-E to that of 304-B shows a similar disparity since at both doses the higher strength 304-B has either the same or lower $(Nd)^{1/2}$ value than that of 304-E. Therefore, even though the same type of defect microstructure exists in each heat, irrespective of it being 304 or 316SS, the Frank loops cannot be considered as a simple obstacle type with an effective 'strength' independent of the material.

A number of possibilities need to be considered to explain the hardening behavior of the Frank loops. First, the materials irradiated in this study contain a number of alloying additions and impurities that can alter the strength through solute strengthening as well as changing the manner in which defects interact with mobile dislocations. Secondly, the RIS alters not just the

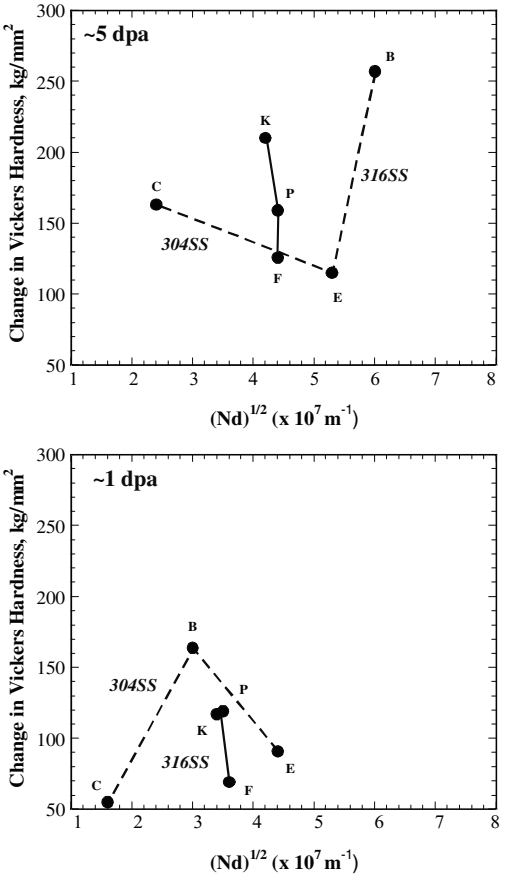

Fig. 12. Comparing the change in hardness at 275 °C versus the $(Nd)^{1/2}$ parameter, where N represents the number density of defects and d represents the average diameter, shows that no clear relationship exists between the defect microstructure and the change in hardness. The data suggest that Frank loops can vary in obstacle strength, possibly due to RIS to the loops and dislocations within the material.

composition of the grain boundaries and near-boundary regions, but also leads to enrichment of Ni and Si (and corresponding depletion of Cr and Fe) at the Frank loops. Kenik [37] reported measuring enrichment at loops in a much earlier study as well. As further evidence of RIS, Shepherd [38] provided convincing evidence of Ni segregating to dislocations in a Nb-stabilized stainless steel under high-energy Ni^{6+} and C^{2+} irradiations. Unfortunately no data is available to indicate how C responds to RIS during neutron irradiation, but this is thought important given the potent effect of C on strengthening and microstructural evolution. Note that in the review by Zinkle et al. [2] and more recently by Lee et al. [27,28] it was stated that RIS is not important at temperatures below 300 °C, but the review by Bruemmer et al. [3,26] shows the opposite to be true. One fact that is not known with certainty, however, is

that the temperature limit below which RIS becomes negligible.

RIS will affect not only the microstructural evolution, but also the manner in which the material deforms since the Frank loops will be locally enriched/depleted in Ni, Si, Cr and Fe and possibly other elements when the doses exceed a few dpa. In other words, a moving dislocation now has to contend with not just Frank loops and other defects, but also with closely spaced, localized regions of compositional variations around the Frank loops, the effect of which is not so easy to quantify. The data presented in this paper indicate that there may be some dependence of hardness on the solute content, and this coupled with RIS to the dislocations and Frank loops may lead to the Frank loops being more effective in one material versus another. To carry this further, the 'effective strength' of the Frank loops may also exhibit a dose dependence in a given material since the composition at the loops changes with the degree of RIS. RIS will also occur at the grain boundaries and any other sinks such as network dislocations, all of which may interact to alter the deformation response.

Precipitation, either in the matrix or on the dislocations and loops, may be another factor that needs to be taken into account. Recent work by Hashimoto et al. [12] indicates that a low density of precipitates form in irradiated stainless steels even at irradiation temperatures as low as 200 °C. The contribution to the strengthening is deemed to be minimal given the precipitate density is a ~1000 times lower than the defects and of similar size. As stated earlier, the only indication of precipitation found in this study was limited evidence of precipitates at 13 dpa in the 316-K at a density similar to that reported by Hashimoto. Edwards et al. [39] found that precipitation does occur at irradiation temperatures of ~320–340 °C, but it is not known if these results extrapolate back to irradiation temperatures of 275 °C. Two types of precipitates were found in their study, one identified as precipitation with a density of $\sim 0.6 \times 10^{23}$ m^{-3} and average size of ~3 nm, and a second unidentified phase of density $\sim 0.2 \times 10^{23}$ m^{-3} and average size of 8.5 nm. Neither of these precipitates appeared to coincide with the existing Frank loops, but there was some evidence that the γ' precipitation may have formed on pre-existing dislocations. In that study, the volume fraction of precipitates was high enough to cause diffraction spots in the diffraction patterns, however, no such evidence was found for precipitation in the present experiment. The limited evidence for radiation-induced precipitation therefore suggests that very fine-scale precipitation may exist, but whether it influences mechanical properties at these doses and irradiation temperatures is uncertain.

The presence of the denuded zones in these materials has been treated previously by Simonen and coworkers [40], and will only be summarized here. The existence of a denuded zone is due to the competing effects of grain boundaries acting as sinks for both vacancies and interstitials versus the buildup of sinks in the matrix. This competition suppresses nucleation of loops or clusters near the boundaries at the low doses until the loop sink strength in the adjacent grain interiors increases to sufficient levels. The differences in width and the general dose dependence when comparing the 304SS and the 316SS alloys remains unexplained, however. One might conjecture that these features are related in some way to the compositional differences of the material and the RIS that occurs, but how these two variables effect nucleation and growth of loops in conjunction with the microstructural evolution near grain boundary regions requires further study.

5. Conclusions

The microstructure of the irradiated stainless steels is comprised of small Frank loops whose size range extends from less than 1–30 nm. The density of visible Frank loops is already established at the lowest dose available in this study for most heats, reaching an average saturation level of $\sim 2 \times 10^{23}$ m^{-3} for the stainless steels in this study. The size distributions continue to change up to doses greater than 5 dpa. The partitioning of the irradiated microstructure into black spots versus Frank loops as is often done in the literature is therefore deemed inappropriate since the black spots are simply small Frank loops.

While the results presented in this study have shown that SFT-like images are fairly common, these defects may simply be the result of asymmetric strain fields around small Frank loops, or in some cases, partially-dissociated Frank loops, a defect configuration intermediate between a Frank loop and an SFT. This study suggests that the Frank loop microstructure is composed of both vacancy and interstitial Frank loops. The only consistent evidence of another defect type was found in the highest purity 304-E, which contained a very low density SFT, which are generally considered to be vacancy in nature.

Impurities and minor solutes appear to influence the microstructural evolution as well as the hardening response. The higher purity heats provide the best evidence of this since they appear to evolve more rapidly in terms of their defect microstructure than the lower purity variants. The hardening behavior reveals that the relationship between the microstructure and hardening is more complex than a simple proportionality between the size and density of the defects versus the increase in strength. As an example, the two higher purity heats of 304 and 316SS exhibit the lowest hardness at 5 dpa despite having the same density of loops and a slightly larger average size compared to the other heats. Frank

loops therefore appear to promote more hardening in certain heats than in others, possibly due to RIS to the loops and other sinks within the material.

Based on the results presented in this study, further investigations are needed to determine the character of the small Frank loops, i.e. vacancy versus interstitial, establish the relative population of the two types of defects if they are present, and study how their stability affects microstructural evolution. Future research is also necessary to evaluate the influence of individual solute elements and RIS on the microstructural evolution and how these factors alter deformation behavior.

Acknowledgements

The authors would like to thank L.E. Thomas, J.S. Vetrano, M.L. Jenkins and M.A. Kirk for insightful discussions during the course of this work. Special thanks are given to Bruce Arey for conducting the hardness testing and Elaine Dieffenbacher for specimen preparation. Support from the internationally sponsored Cooperative IASCC Research Program managed by EPRI, from the Materials Science Division of the Office of Basic Energy Sciences and from the Office of Nuclear Energy, Science and Technology, US Department of Energy under contract DE-AC06-76RLO 1830 is gratefully acknowledged.

References

[1] P. Maziasz, J. Nucl. Mater. 205 (1993) 118.
[2] S.J. Zinkle, P. Maziasz, R.E. Stoller, J. Nucl. Mater. 206 (1993) 266.
[3] S.M. Bruemmer, E.P. Simonen, P.M. Scott, P.L. Andresen, G.S. Was, J.L. Nelson, J. Nucl. Mater. 274 (1999) 299.
[4] A.F. Rowcliffe, S.J. Zinkle, J.F. Stubbins, D.J. Edwards, D.J. Alexander, J. Nucl. Mater. 258–263 (1998) 183.
[5] H.R. Brager, J.L. Straalsund, J. Nucl. Mater. 46 (1973) 134.
[6] H.R. Brager, E.R. Gilbert, J.L. Straalsund, Radiat. Eff. 21 (1974) 37.
[7] B.L. Eyre, Fundamental Aspects of Radiation Damage in Metals, 2, in: M.T. Robinson, F.W. Young Jr. (Eds.), CONF-751006-P2, NTIS, Springfield, VA,1975, p. 1196.
[8] T. Muroga, Y. Miyamoto, H. Watanabe, N. Yoshida, J. Nucl. Mater. 155–157 (1988) 810.
[9] M. Horiki, M. Kiritani, J. Nucl. Mater. 212–215 (1994) 246.
[10] E.H. Lee, J.D. Hunn, T.S. Byun, L.K. Mansur, J. Nucl. Mater. 280 (2000) 18.
[11] E.H. Lee, J.D. Hunn, N. Hashimoto, L.K. Mansur, J. Nucl. Mater. 278 (2000) 266.
[12] N. Hashimoto, E. Wakai, J.P. Robertson, J. Nucl. Mater. 273 (1999) 95.
[13] N. Yoshida, J. Nucl. Mater. 174 (1990) 220.
[14] S.M. Bruemmer, D.J. Edwards, B.W. Arey, L.A. Charlot, 9th Int. Symp. Environmental Degradation of Materials in Nuclear Power Systems – Water Reactors, NACE, 1999, p. 1079.
[15] Y. Dai, X. Jia, J.C. Chen, W.F. Sommer, M. Victoria, G.S. Bauer, J. Nucl. Mater. 296 (2001) 174.
[16] C. Bailat, A. Almazouzi, N. Baluc, R. Schäublin, F. Gröschel, M. Victoria, J. Nucl. Mater. 283–287 (2000) 446.
[17] C. Bailat, F. Gröschel, M. Victoria, J. Nucl. Mater. 276 (2000) 283.
[18] J.T. Busby, T.R. Allen, J. Gan, G.S. Was, E.A. Kenik, in: Proc. Eighth Int'l Symp. Environmental Degradation of Materials in Nuclear Power Systems – Water Reactors, American Nuclear Society, La Grange Park, IL, 1997, p. 758.
[19] G.S. Was, J.T. Busby, J. Gan, E. Kenik, A. Jenssen, S. Bruemmer, P. Scott, P. Andresen, D.J. Edwards, J. Nucl. Mater. 300 (2002) 198.
[20] D.J. Edwards, E.P. Simonen, S.M. Bruemmer, in: S.M. Bruemmer, P. Ford, G. Was (Eds.), 9th International Symposium on Environmental Degradation of Materials in Nuclear Power Systems – Water Reactors, The Minerals, Metals and Materials Society, Pennsylvania, 1999, p. 1007.
[21] D.J. Edwards, E.P. Simonen, S.M. Bruemmer, Mat. Res. Soc. Symp. Proceedings, 650, 2000, R2.7.1.
[22] A. Jenssen, L.G. Ljungberg, 7th Int. Symp. Environmental Degradation of Materials in Nuclear Power Systems – Water Reactors, NACE, 1995, p. 1043.
[23] A. Jenssen, L.G. Ljungberg, K. Pettersson, J. Walmsley, 8th Int. Symp. Environmental Degradation of Materials in Nuclear Power Systems – Water Reactors, NACE, 1997, p. 785.
[24] B.M. Oliver, F.A. Garner, L.R. Greenwood, J. Nucl. Mater. 283–287 (2000) 1006.
[25] M.L. Jenkins, M.A. Kirk, in: Characterization of radiation damage by transmission electron microscopy, Institute of Physics, Bristol and Philadelphia, 2001, p. 58.
[26] S.M. Bruemmer, D.J. Edwards, V.Y. Gertsman, E.P. Simonen, Mat. Res. Soc. Symp. Proceedings, 650, 2000, R2.1.1.
[27] E.H. Lee, T.S. Byun, J.D. Hunn, M.H. Yoo, K. Farrell, L.K. Mansur, Acta Mater. 49 (2001) 3269.
[28] E.H. Lee, M.H. Yoo, T.S. Byun, J.D. Hunn, K. Farrell, L.K. Mansur, Acta Mater. 49 (2001) 3277.
[29] J.P. Hirth, J. Lothe, in: Theory of Dislocations, 2nd ed., Krieger Publishing Company, Wiley, 1992, p. 323.
[30] W. Schilling, J. Nucl. Mater. 69&70 (1978) 465.
[31] E.P. Simonen, S.M. Bruemmer, J. Nucl. Mater. 239 (1996) 185.
[32] N.Q. Lam, A. Kumar, H. Wiedersich, in: H.R. Brager, J.S. Perrin (Eds.), 11th International Symposium on the Effects of Radiation on Materials, ASTM STP 782, ASTM, 1982, p. 985.
[33] H. Fukushima, Y. Shimomura, J. Nucl. Mater. 205 (1993) 59.
[34] Y. Miwa, T. Tsukada, S. Jitsukawa, S. Kita, S. Hamada, Y. Matsui, M. Shindo, J. Nucl. Mater. 233–237 (1996) 1393.
[35] T. Tsukada, T. Kondo, Proceedings of the 8th International Symposium on Environmental Degradation in Nuclear Power Systems – Water Reactors, 2, 1997, p. 795.

[36] E. Orowan, in: Internal Stresses in Metals and Alloys, Institute of Metals, London, 1948, p. 451.
[37] E.A. Kenik, Scr. Metall. 10 (1976) 735.
[38] C.M. Shepherd, J. Nucl. Mater. 175 (1990) 170.
[39] D.J. Edwards, E.P. Simonen, F.A. Garner, S.M. Bruemmer, J. Nucl. Mater. 317 (2003) 32.
[40] E.P. Simonen, D.J. Edwards, S.M. Bruemmer, in: S.M. Bruemmer, P. Ford, G. Was (Eds.), 9th International Symposium on Environmental Degradation of Materials in Nuclear Power Systems – Water Reactors, The Minerals, Metals and Materials Society, Pennsylvania, 1999, p. 1107.